

Quercetin-Loaded Luminescent Hydroxyapatite Nanoparticles for Theranostic Application in Monolayer and Spheroid Cultures of Cervical Cancer Cell Line *In Vitro*

Anitha T. Simon, Deepanjalee Dutta, Arun Chattopadhyay,* and Siddhartha Sankar Ghosh*

Cite This: <https://doi.org/10.1021/acsabm.1c00255>

Read Online

ACCESS |



Metrics & More



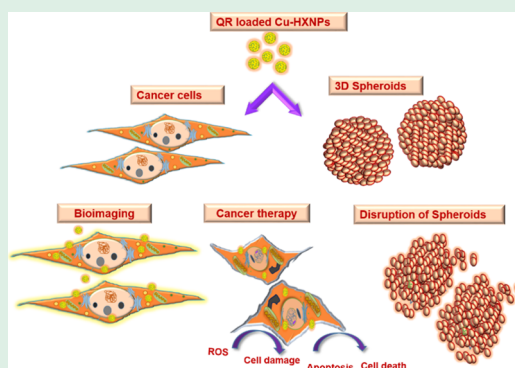
Article Recommendations



Supporting Information

ABSTRACT: Nanoscale materials have been explored as better alternatives to conventional therapeutic agents in cancer theranostics in the recent period due to efficacy in overcoming biological, biomedical, and biophysical barriers. Analysis on the ability of copper nanocluster (CuNC)-doped hydroxyapatite nanoparticles (Cu-HXNPs) as suitable nanocarriers for anticell proliferative application was carried out. Having high adsorption capacity, the Cu-HXNPs could be loaded with the anticancer drug quercetin, which is a polyphenolic flavonoid compound, and were used as nanocarriers to be applied on HeLa (cancer cells) and HEK-293 (normal cells). The drug release profile was found to be pH-dependent, where maximum release of quercetin from quercetin-loaded Cu-HXNPs was observed in acidic pH as compared to physiological pH. The Cu-HXNPs could release quercetin, which could effectively decline proliferation of cancer cells via generation of reactive oxygen species. Moreover, the released quercetin significantly altered the cell cycle pattern and triggered the cells to undergo apoptosis. Additionally, the efficacy of Cu-HXNPs as a nanocarrier to release quercetin on 3D spheroids of HeLa had been checked, which demonstrated significant reduction in the viability of 3D spheroids. The luminescent CuNCs used for doping HXNPs endowed the nanocarrier with the imaging property, which was an excellent feature in confirming their uptake by the cells. Thus, the study suggested Cu-HXNPs to be a beneficial nanocarrier for both bioimaging and therapeutic purpose in the field of cancer theranostics.

KEYWORDS: *theranostics, hydroxyapatite, quercetin, 3D spheroids, bioimaging*



INTRODUCTION

The amalgamation of diverse scientific disciplines has expedited the generation of novel medicines bridging science and clinical applications, resulting in the emergence of the field of nanomedicines.¹ The area of cancer nanomedicine is aimed to address a majority of pharmacological limitations of conventional drugs. Nanoformulation of naturally or synthetically derived materials has been found to be effective for attaining cancer therapy using them as drug delivery vehicles. Both organic and inorganic nanomaterials can be engineered for encapsulating therapeutic drugs, whose tumoricidal property remains unaltered.^{2,3} The organic-based nanocarriers include polymeric, dendrimeric, cell membrane-derived, lipid and carbon-based platforms, whereas inorganic counterparts comprise iron oxide, gold, copper, silver, silica, and hydroxyapatite (HXAp). Intensive investigations of inorganic nanocarriers have been widely conducted due to their favorable surface properties, appreciable drug loading capacity, minimal toxicity, bioavailability, controlled or sustained drug release, and stability toward organic solvents.^{4–6}

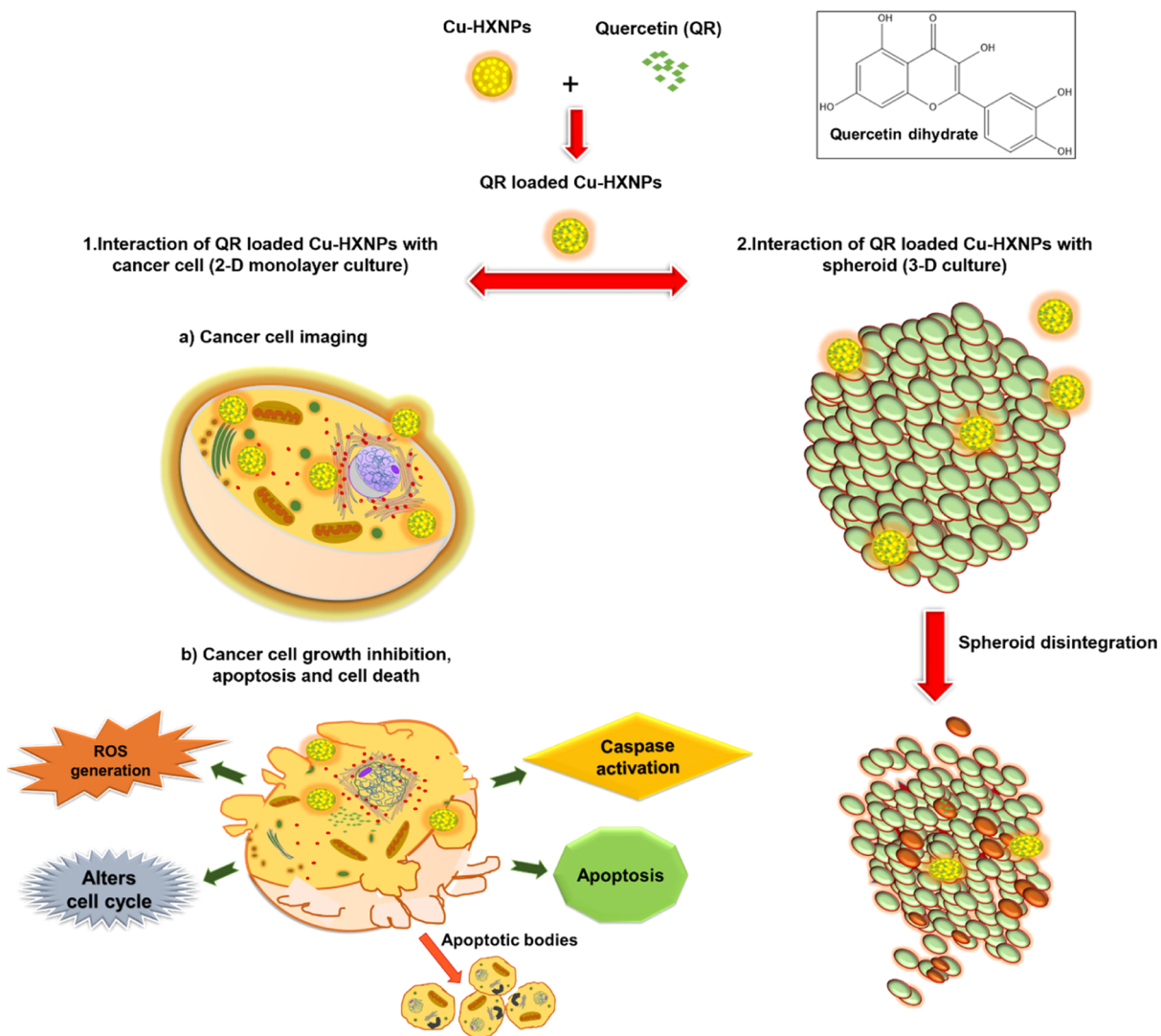
Due to the structural and compositional similarities with biological tissues such as bone and teeth, HXAp has been

extensively considered for medical applications. In general, nanoparticles inherit salient features as compared to their bulk counterparts in terms of their reactivity, surface reconstruction, structure-related sensitivity, and adsorption property. Similarly, the nanostructured HXAp material possesses a higher surface area, biocompatibility, high adsorption property, and higher affinity for chemical species. These inherent nanoscale properties of HXAp can be exploited for drug delivery application in cancer nanomedicines.^{7–10} Integration of the bioimaging property into therapy is an effective approach in monitoring and interpretation of the mode and site of nanocarrier distribution. Based on luminescence, probing of the therapy can be achieved through the usage of quantum dots, carbon nanomaterials, upconversion nanoparticles, metal

Received: February 28, 2021

Accepted: April 14, 2021

Scheme 1. Schematic Representation of Quercetin Loading Into Cu-HXNPs Followed by Bioimaging and Therapeutic Application in Cancer Cells Such as 2D Monolayer Culture and 3D Spheroids of HeLa⁴



⁴The structure of quercetin dihydrate is shown (inset).

nanoclusters, and incorporation of fluorescent dyes.^{11,12} Out of these, metal nanoclusters are a new class of emerging fluorophores having a size closely approaching to Fermi wavelength of electrons and possess discrete energy levels. Among nanoclusters, copper nanoclusters (CuNCs) have attained substantial attention due to their size-tunable luminescent emission between near UV to near-infrared region, water solubility, high photoluminescence, and negligible renal retention.^{13–15} Using CuNCs, image-guided therapeutic analysis can be achieved with negligible cytotoxicity after incorporating them into biocompatible nanomaterials such as HXAp.¹⁶

Among the naturally occurring compounds, polyphenols are a group of therapeutically important agents toward treatment of various disease conditions. Quercetin among them is uniquely positioned due to its anticell proliferative nature, intrinsic potency of angiogenesis inhibition, and apoptosis. However, its pharmaceutical usages have been limited due to poor bioavailability and poor water solubility. Therefore, it is essential to harness its applications using an effective strategy

such as loading it to suitable drug delivery vehicles for cancer therapy.^{17–19}

Herein, we report the loading of quercetin into CuNC-doped HXAp nanoparticles (Cu-HXNPs) for checking the potentiality of the nanocarrier in releasing the anticancer drug to be applied effectively for anticell proliferative activity. Being a suitable host, HXNPs could be successfully doped with CuNCs, with further loading of quercetin.^{16,20} About 72% of quercetin could be loaded into Cu-HXNPs. The quercetin-loaded Cu-HXNPs after interacting with HeLa cells inhibited their growth via triggered generation of reactive oxygen species (ROS). Doping with metal ions such as copper could enhance the clinical effect of anticancer drugs such as quercetin through HXNPs, with the generation of ROS, leading to oxidative damage, probably through the transition-metal based pathway.^{21,22} Moreover, with the aid of Cu-HXNPs as nanocarriers, the ROS generation through transition metal-flavone complexation could induce apoptosis, possibly via altering the mitochondrial membrane function.^{23–25} Importantly, the cell cycle pattern was affected and eventual apoptosis killed the treated HeLa cells. While investigating the effect of quercetin-

loaded Cu-HXNPs on the viability of the HEK-293 cell line, minimal growth inhibition was observed at lower concentrations with gradual reduction in cell viability toward higher concentrations. Importantly, the current study has also included the employment of 3D spheroids of the HeLa cell line, which bridge the gap between the 2D monolayer culture and animal model and mimic the tumor microenvironment *in vivo*²⁶ (Scheme 1). The luminescent property of quercetin-loaded Cu-HXNPs also aided in confirmation of cellular uptake of the entire nanocarrier.

MATERIALS AND METHODS

Chemicals. For the experimental purpose, the following chemicals were used as-purchased: calcium chloride dihydrate (Merck), strontium nitrate pure (Merck), potassium dihydrogen phosphate (Merck), poly ethylene glycol (PEG) 400 (Merck), polyvinyl alcohol 87–89% hydrolyzed (Sigma-Aldrich), glacial acetic acid (Rankem), ammonia 25% (Merck), copper(II) sulfate pentahydrate pure (Merck), bovine serum albumin (Himedia), sodium hydroxide pellet (Rankem), hydrazine hydrate 80% (Merck), quercetin dihydrate (Sisco Research Laboratories), and dimethyl sulfoxide (DMSO, Merck). Milli-Q grade water ($>18\text{ M}\Omega\text{ cm}^{-1}$, Millipore) was used in all the experiments.

Synthesis of HXNPs (Undoped HXNPs), CuNCs, and CuNC-Doped HXNPs (Cu-HXNPs). The entire synthesis procedures have been adopted from our previous report¹⁶ out of which, synthesis of CuNC-doped HXNPs (Cu-HXNPs) has been explained briefly here.

To synthesize Cu-HXNPs, in 3 mL of water, 0.2 M calcium chloride dihydrate and 0.12 M strontium nitrate were mixed and 7 mL of PEG 400 was added and stirred. The pH was brought to 11, followed by the addition of synthesized CuNC dispersion. Furthermore, 3 mL of 0.12 M potassium dihydrogen phosphate was added. The first set of dispersion was mixed with the second set of poly(vinyl alcohol) solution containing 2.5% diluted glacial acetic acid and 0.5% ammonia, whose pH was already adjusted to 11. Finally, the whole reaction mixture was heated at 85 °C for 2 min. After the synthesis, centrifugation was carried out twice at 5000 rpm. The final dispersion was stored at 4 °C for experimental purpose.

Drug Loading Efficiency. To check the quercetin loading efficiency of Cu-HXNPs, 500 μL of 5 mM quercetin was added to 500 μL of Cu-HXNPs (having a calcium concentration of 0.76 mg/mL) and incubated for 2 h at 37 °C. After incubation, centrifugation was carried out at 5000 rpm for 5 min to remove the supernatant. The pellet was dispersed in 1 mL of water, and the loading efficiency was checked using fluorescence spectroscopy (PerkinElmer LS55 spectrofluorometer). The fluorescence was recorded at an excitation and emission wavelength of 370 and 535 nm respectively. Using the following formula, the loading efficiency was calculated.

$$\% \text{ of loading efficiency} = \frac{QR_i - QR_f}{QR_i} \times 100$$

Here, QR_i denotes the initial concentration of quercetin used for loading and QR_f denotes the concentration of quercetin in the supernatant.

Study on Quercetin Release from Cu-HXNPs. The quercetin release profile was carried out in pH 4 (acetate buffer) and pH 7.4 [phosphate-buffered saline (PBS) buffer]. After the addition of 500 μL of 5 mM quercetin into 500 μL of Cu-HXNPs, incubation was conducted for 2 h at 37 °C. Following the incubation, centrifugation was carried out at 5000 rpm for 5 min and the supernatant was removed. After dispersing the pellet in different pH buffers, release study was performed and the samples were periodically removed at different time intervals (0th, 3rd, 6th, 9th, 12th, 24th, 36th, 48th, 72nd, and 96th h). Furthermore, the withdrawn samples were centrifuged and their supernatant was collected to analyze the release profile by fluorescence spectroscopy. The fluorescence measurements were taken at an excitation of 370 nm and at an emission of 535 nm.

The cumulative release was calculated using the formula given as follows.

$$\text{Cumulative release \%} = \frac{\text{QR released in supernatant}}{\text{QR loaded in nanocarrier}} \times 100$$

UV-Visible Spectroscopy. A UV-visible spectrophotometer (Jasco V-630) was used to record the absorbance profile of quercetin, quercetin-loaded Cu-HXNPs, Cu-HXNPs, HXNPs, and CuNCs in the UV-visible range.

Luminescence Measurements. All the luminescence measurements were conducted using a fluorescence spectrophotometer (using a PerkinElmer LS55 spectrofluorometer and Fluorolog Horiba). Time-resolved photoluminescence (TRPL) analysis was carried out for CuNCs and Cu-HXNPs using a FluroMax-4 spectrofluorometer.

TEM. The as-synthesized CuNCs, undoped HXNPs, Cu-HXNPs, and sample was analyzed under a transmission electron microscope, having a maximum accelerating voltage of 200 keV (JEM 2100; JEOL, Peabody, MA). Transmission electron microscopy (TEM) imaging was carried out by drop-casting 7 μL of the sample to a carbon-coated copper grid. The sample was air-dried overnight. Prior to drop-casting, the sonicated in an ultrasonic bath (Telsonic) for 40 min.

FESEM. To study the morphology of quercetin-loaded Cu-HXNPs and undoped HXNPs, field emission scanning electron microscopy (FESEM) (JEOL JSM-7610F) was conducted. About 20 μL of the sample was drop-casted to an aluminum foil-covered glass slide and air-dried overnight. Before drop-casting, sonication of the sample was carried out for 40 min.

To understand the cell surface morphology, the treated and control cells of HeLa and HEK-293 were imaged using FESEM. For analysis, the cells (HeLa or HEK-293) were treated with quercetin-loaded Cu-HXNPs. Incubation of both treated and control cells was carried out at 37 °C for 24 h. Furthermore, the cells were washed using PBS and trypsinized. The fixation of the cells was carried out with 0.1% formaldehyde followed by washing the cells with PBS. To an aluminum foil-covered glass slide, 20 μL of the diluted culture was drop-casted and air-dried overnight.

Zeta Potential. The zeta potential of Cu-HXNPs, quercetin, and quercetin-loaded Cu-HXNPs was recorded using a Malvern Zetasizer Nano ZS.

LCMS. Using liquid chromatography mass spectrometry (LCMS) (Q-ToF premier), the interaction of quercetin with Cu-HXNPs was studied. The analysis was carried out for quercetin and quercetin-loaded Cu-HXNPs.

STUDIES ON CELLULAR ACTIVITIES

Cell Culture. For performing cell culture studies, HeLa (human cervical carcinoma) and HEK-293 (human embryonic kidney-293) cells were procured from National Centre for Cell Sciences (NCCS), Pune, India. For culturing the cells, Dulbecco's modified Eagle's medium (DMEM) supplemented with L-glutamine (4 mM), penicillin (50 units per mL), streptomycin (50 mg/mL, Sigma-Aldrich), and fetal bovine serum (10% v/v, PAA Laboratories, Austria) was used. The cells were grown in a 5% CO₂ humidified incubator at 37 °C.

Cell Viability Assay. The cell viability assay using MTT [3-(4,5-dimethylthiazol-2-yl)-2,5-diphenyltetrazolium bromide] was carried out on HeLa cells and HEK-293 (normal cell line). For the assay, 1×10^4 HeLa or HEK-293 cells/well were seeded into a 96-well plate and cultured in DMEM media inside a 5% CO₂-humidified incubator overnight at 37 °C for 24 h. The cells were treated with Cu-HXNPs (quercetin concentration, 0 μM) and quercetin-loaded Cu-HXNPs of varying quercetin concentrations (ranging from 100 to 500 μM) and quercetin (concentrations ranging from 100 to 500 μM) and incubated at 37 °C for 48 h. For the entire study, quercetin was dissolved in DMSO with the concentration of DMSO not exceeding 0.1% in cell culture medium. At the end

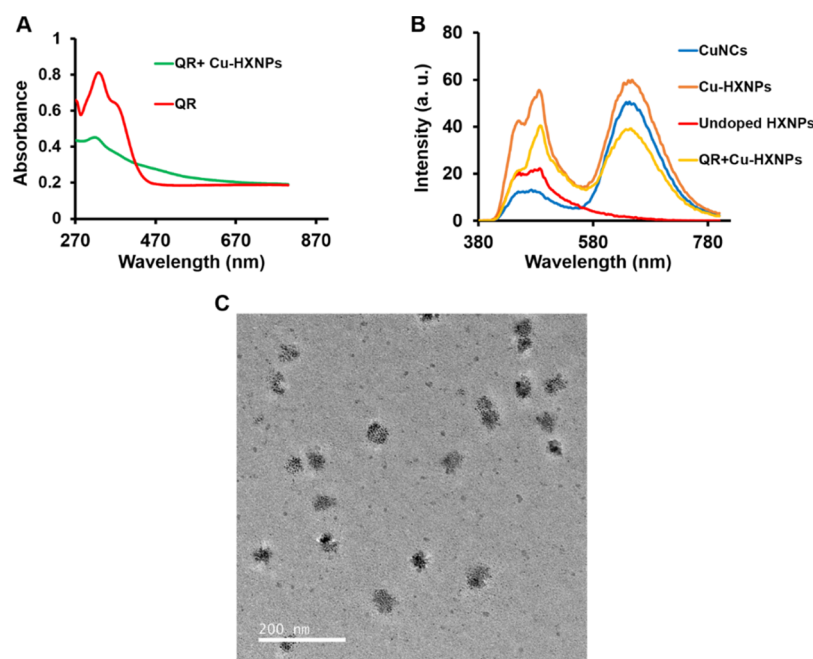


Figure 1. (A) UV–visible absorption spectra of quercetin (QR)-loaded Cu-HXNPs and free quercetin. (B) Emission spectra of CuNCs, Cu-HXNPs, undoped HXNPs, and quercetin-loaded Cu-HXNPs with their emission peaks at 650 nm (excitation at 365 nm). (C) TEM image of quercetin-loaded Cu-HXNPs at a scale bar of 200 nm.

of 48 h treatment, the MTT assay was carried out. The respiratory mitochondrial enzyme in the live cells reduces MTT to the formazan product which can be detected spectrophotometrically at 570 nm with the reference filter at 655 nm. The amount of formazan formed is directly proportional to the number of live cells. The percentage (%) of cell viability was calculated as follows.

$$\% \text{ of viable cells} = \frac{(A_{570} - A_{655})_{\text{of treated cells}}}{(A_{570} - A_{655})_{\text{of control cells}}} \times 100$$

Generation of 3D Spheroids. Initially, HeLa cells were grown as monolayers until confluency was obtained, followed by trypsinization and resuspension in DMEM media. For the formation of spheroids, the 96-well plates were pre-coated with 1.5% agarose-containing serum-free DMEM media. Once solidified, HeLa cells at a density of 15,000 cells per well were seeded followed by centrifuging at 700 rcf for 10 min. Furthermore, the 96-well plates were incubated at 37 °C inside a 5% CO₂ humidified incubator for 96 h. Once the generation of spheroids is achieved, they were used for further studies.

Viability Study on 3D Spheroids. The viability study was carried out by treating spheroids with Cu-HXNPs (quercetin concentration, 0 μM) and quercetin-loaded Cu-HXNPs of varying quercetin concentrations (ranging from 200 to 1000 μM) and quercetin (concentrations ranging from 200 to 1000 μM) for 48 h at 37 °C. At the end of treatment, the viability was assessed using almarBlue assay by recording the absorbance at 570 nm, fixing the reference filter at 655 nm. The cell viability (%) was determined using the given formula.

$$\% \text{ of viable cells} = \frac{(A_{570} - A_{655})_{\text{of treated cells}}}{(A_{570} - A_{655})_{\text{of control cells}}} \times 100$$

Confocal Laser Scanning Microscopy. The confocal experiment was carried out by treating the HeLa cells with Cu-HXNPs, quercetin-loaded Cu-HXNPs, and free quercetin at

the IC₅₀ concentration of quercetin-loaded Cu-HXNPs and incubating for 3 h at 37 °C. The samples were viewed under a Zeiss LSM 880 microscope (at a laser excitation of 405 nm).

For understanding the subcellular localization property, lysosomal staining assay was conducted using a cytopainter green lysosomal staining kit (Abcam). After the treatment of HeLa cells with quercetin-loaded Cu-HXNPs for 3 h, manufacturer's instructions were followed, where staining was carried out for one and half hour. The fixed cells were further visualized at an excitation of 405 nm (quercetin loaded Cu-HXNPs) and 488 nm (cytopainter green).

In the case of spheroids, live/dead cell imaging was carried out using the acridine orange/propidium iodide staining method. After being subjected to treatment with Cu-HXNPs, quercetin-loaded Cu-HXNPs, and free quercetin for 48 h, the spheroids were viewed under a Zeiss LSM 880 microscope. The treatment of spheroids with the given samples was carried out at a concentration in which quercetin-loaded Cu-HXNPs exerted 50% (approx.) viability reduction.

Determination of ROS Generation. The ROS generation from the cells treated with Cu-HXNPs, quercetin-loaded Cu-HXNPs, and free quercetin was studied using a microplate reader (Tecan) and epi-fluorescence microscopy (Nikon ECLIPSE, TS100, Tokyo). Primarily, the treatment of cells with quercetin-loaded Cu-HXNPs and free quercetin was carried out in a 96-well plate for 3 h. By the completion of the treatment, the cells were incubated with 1 mM DCFH-DA (2,7-dichlorofluoresceindiacetate) for 10 min. The cells were replenished with fresh media. The nonfluorescent DCFH-DA after the diffusion into the cells is hydrolyzed to DCFH, which upon oxidation gets converted into green-emitting DCF (dichlorofluorescein). The ROS generation was confirmed at an excitation of 488 nm and an emission of 530 nm.

Cell Cycle Analysis. For cell cycle analysis, HeLa cells (1 × 10⁵ cells) were seeded in a six-well plate. The grown cells were treated with Cu-HXNPs, quercetin-loaded Cu-HXNPs, and

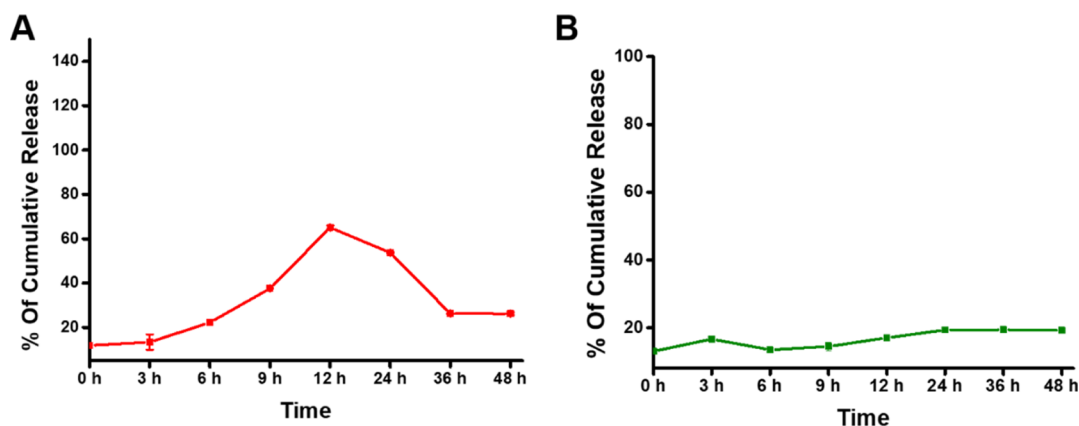


Figure 2. Study on the release pattern of quercetin from quercetin-loaded Cu-HXNPs carried out at (A) pH 4 (acetate buffer) and (B) pH 7.4 (PBS buffer). At pH 4, an initial burst release of 65% was obtained at 12th h followed by 53% of release at 24th h. Toward 48th h, the drug release was gradually reduced to 26% in a slow and sustained manner. The release profile of quercetin at pH 7.4 exhibited initially a maximum release of 17% at 12th h, with a slow increase to 19% of release at 48th h.

free quercetin for 48 h. After the completion of the treatment, the media and the PBS of both control and treated cells were separately collected and the cells were trypsinized. The media, PBS, and the trypsinized cells were centrifuged at 650 rcf for 5 min, and cells were collected. Under constant and careful vortexing, the cells were fixed using 70% of ice cold ethanol and stored at 4 °C. Furthermore, the cells were centrifuged and washed using ice cold PBS after which they were treated with RNase for 1 h at 55 °C. To the RNase-treated cells, 10 μ L of PI (1 mg/mL) was added and incubated in the dark at 37 °C for 30 min. Finally, all the samples were analyzed in a FACS Calibur (BD Biosciences, NJ) flow cytometer. For each sample, 15000 cells were analyzed for recording PI fluorescence using the CellQuest program (BD Biosciences).

Cleaved Caspase 3 Assay. Here, HeLa cells (1×10^5 cells) were grown and treated with Cu-HXNPs, quercetin-loaded Cu-HXNPs, and quercetin for 48 h. The control and treated cells were trypsinized and centrifuged at 650 rcf for 5 min. Using 0.1% formaldehyde, the cells were fixed for 15 min. The fixed cells were centrifuged, and the pellet was redispersed in PBS. Upon the addition of 0.5% Tween 20, the cells were incubated in the dark for 20 min. Thereafter, the cells were centrifuged and washed thrice using PBS. Furthermore, 10 μ L of the PE-conjugated anticaspase-3 antibody was added, and the cells were incubated at 37 °C for 30 min. The cleaved caspase 3 assay was carried out in a FACS Calibur flow cytometer (BD Biosciences, NJ). Fluorescence data of every sample were recorded for 15000 cells through the CellQuest program (BD Biosciences).

RESULTS AND DISCUSSION

The as-synthesized Cu-HXNPs were loaded with anticancer drug quercetin. The loading of quercetin into Cu-HXNPs was further confirmed by UV–visible and fluorescence spectroscopy methods. UV–visible spectroscopy revealed the presence of a peak at around 330 nm and 332 nm in the case of quercetin-loaded Cu-HXNPs and free quercetin, respectively. A weaker peak at 377 nm was also observed in the case of free quercetin (Figure 1A). A weak shoulder at 377 nm further supported the incorporation of quercetin in the Cu-HXNPs. This concurs with the earlier reports, which suggest that quercetin has an absorption peak in the range between 320 and 380 nm.²⁷ Furthermore, the analysis on CuNCs and Cu-

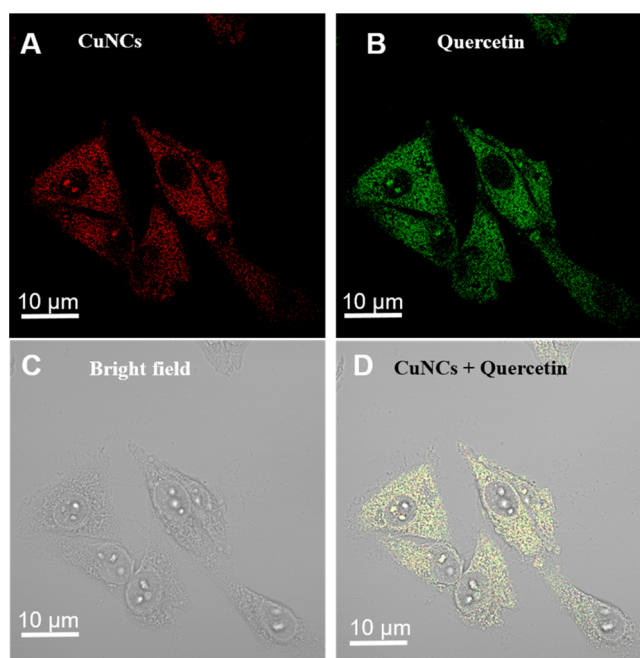


Figure 3. Confocal images showing HeLa cell uptake of quercetin-loaded Cu-HXNPs. (A) Confocal image of HeLa cells treated with quercetin-loaded Cu-HXNPs (emission at 650 nm that corresponds to CuNCs doped in HXNPs) and (B) confocal image of quercetin-loaded Cu-HXNP-treated HeLa cells (emission set at 530 nm that corresponds to quercetin). (C) Bright field image of HeLa cells treated with quercetin-loaded Cu-HXNPs and (D) merged image of HeLa cells treated with quercetin-loaded Cu-HXNPs. The HeLa cells were treated at IC_{50} concentration of quercetin-loaded Cu-HXNPs. The laser excitation was kept at 405 nm. The scale bar is 10 μ m.

HXNPs through UV–visible spectroscopy signified the presence of a peak at around 280 nm corresponding to the bovine serum albumin (BSA) template present in CuNCs. No surface plasmon resonance peak was found in the visible region discounting the formation of bigger-sized copper nanoparticles in both CuNCs and Cu-HXNPs. Additionally, no significant peak was observed throughout the scanned range in the case of HXNPs (Figure S1A). When quercetin-loaded Cu-HXNPs were excited at 370 nm, a sharp emission peak at 490 nm and a broader peak at around 535 nm attributed to quercetin were

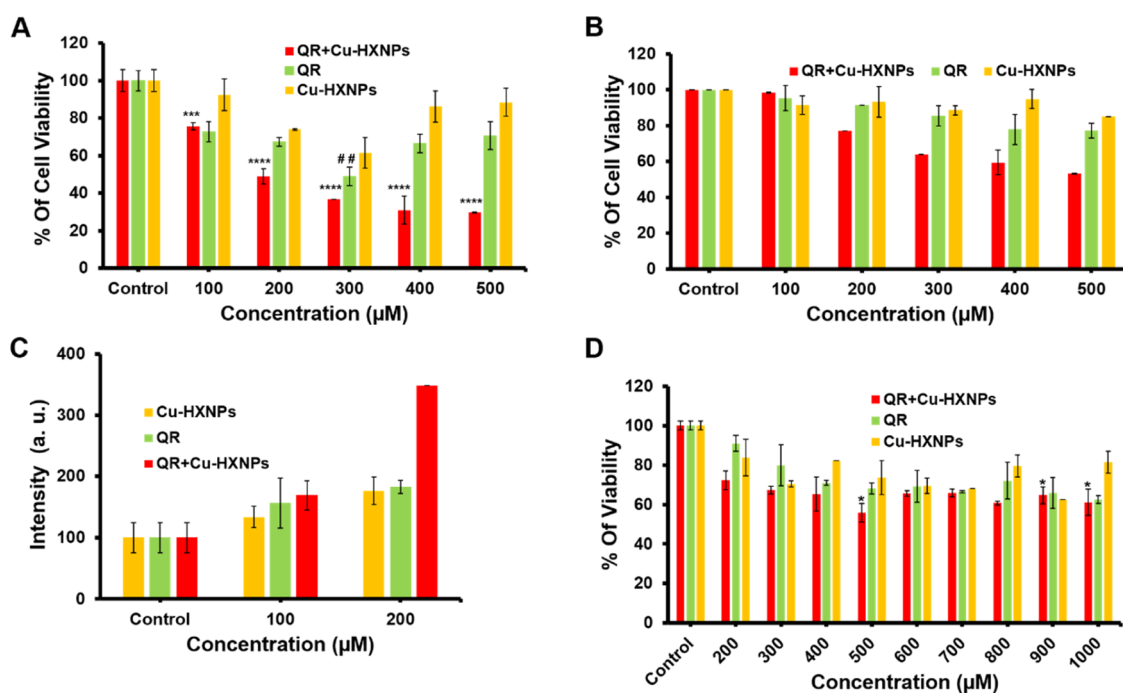


Figure 4. (A) Cell viability assay on HeLa cells treated with quercetin-loaded Cu-HXNPs, free quercetin, and Cu-HXNPs. At a concentration of 200 μM quercetin, quercetin-loaded Cu-HXNPs showed their IC_{50} , whereas free quercetin showed an IC_{50} at 300 μM . The ANOVA test revealed statistical significance of quercetin-loaded Cu-HXNPs and free quercetin with respect to the control. Statistical significance is represented by ## ($p < 0.005$), *** ($p < 0.001$), and **** ($p < 0.0001$). The values are represented as mean \pm standard deviation (SD) of three individual experiments. (B) Viability assay on HEK-293 cells treated with quercetin-loaded Cu-HXNPs, free quercetin, and Cu-HXNPs. Data represented are based on three separate experiments conducted. (C) Graph representing the intensity of ROS generation in HeLa cells treated with Cu-HXNPs, free quercetin, and quercetin-loaded Cu-HXNPs. The graph depicts the averaged intensity value from triplicate experiments. (D) Viability assay on 3D spheroids after the treatment with quercetin-loaded Cu-HXNPs, free quercetin, and Cu-HXNPs. Upon treatment of spheroids with quercetin-loaded Cu-HXNPs, approximately 50% viability reduction was observed at 500 μM quercetin. Statistical significance of quercetin-loaded Cu-HXNPs with respect to the control is denoted by * ($p < 0.05$). Data are represented as mean \pm SD of three individual experiments.

observed.²⁸ In the case of free quercetin, emission peaks at 490 and 540 nm were observed (Figure S1B,S1C). Moreover, at an excitation of 365 nm, the CuNCs, Cu-HXNPs, and quercetin-loaded Cu-HXNPs exhibited an emission peak around 650 nm that attributes to CuNCs. A slight reduction in the fluorescence intensity of quercetin-loaded Cu-HXNPs was observed, probably due to the covalent binding of quercetin with BSA protein, which was used as a template in CuNCs.²⁹ In the case of undoped HXNPs, fluorescence emission was negligible at 650 nm (Figure 1B). At an excitation of 370 nm, quercetin exhibited an emission wavelength in a range of 535–540 nm, which is not inclusive within the red region of the visible spectrum. Therefore, the red fluorescence-emitting CuNCs, doped in Cu-HXNPs, can be specifically applied in the imaging of biological cells and tissue. An emission obtained in the region of such a longer wavelength not only permits deeper tissue penetration but also diminishes autofluorescence from the cellular milieu.³⁰ Being a bioimaging material, to further understand the intrinsic property of our nanocarrier, a TRPL analysis (TRPL) was conducted. The study indicated the lifetime of CuNCs to be 4.25 μs , whereas Cu-HXNPs were found to have an average lifetime of 5.37 μs . The lifetime of both CuNCs and Cu-HXNPs was recorded at an excitation/emission of 365/650 nm (Figure S2).

Furthermore, the TEM analysis revealed the quercetin-loaded Cu-HXNPs to be having an average size of 36.2 ± 4.3 nm (Figure 1C). Likewise, the average size of Cu-HXNPs, HXNPs, and CuNCs was calculated to be 32.2 ± 5.9 , 24.2 ± 6.0 , and 1.7 ± 0.7 nm respectively (Figure S3A–C). Size

calculations of nanoparticles and nanoclusters were carried out using Image J software. The selected area electron diffraction patterns obtained suggested the crystalline nature of the quercetin-loaded Cu-HXNPs with planes (210) and (420) that correspond to the planes of HXNPs as previously reported³¹ (Figure S4A). Thus, it implies that the crystalline properties of Cu-HXNPs were found to be unaltered and intact even after having the quercetin loaded into them. Similarly, the high-resolution TEM image also suggested the presence of lattice spacing of 0.47 nm that corresponds to the (110) plane of HXAp^{32,33} (Figure S4B).

Additionally, the FESEM images obtained were in accordance with the TEM results where the size of the quercetin-loaded Cu-HXNPs was found to be 36.0 ± 8.9 nm. The FESEM analysis suggested the undoped HXNPs to be having an average size of 24.5 ± 2.8 nm, which corresponds to the TEM images of undoped HXNPs (Figure S5A,B). The energy-dispersive X-ray spectroscopy (EDX) confirmed the presence of individual ions such as calcium, phosphorous, strontium, copper, carbon, and oxygen in quercetin-loaded Cu-HXNPs (Figure S6).

For the determination of surface charges, the zeta potential analysis was conducted, which confirmed that the quercetin-loaded Cu-HXNPs carried a net negative charge of -20.5 ± 0.2 mV (Figure S7A). The free quercetin and Cu-HXNPs carried net negative charges of -39.1 ± 0.3 and -19.3 ± 0.1 mV, respectively (Figure S7B,C). The interaction of negatively charged quercetin and negatively charged Cu-HXNPs might be probably due to the influence of positively charged calcium

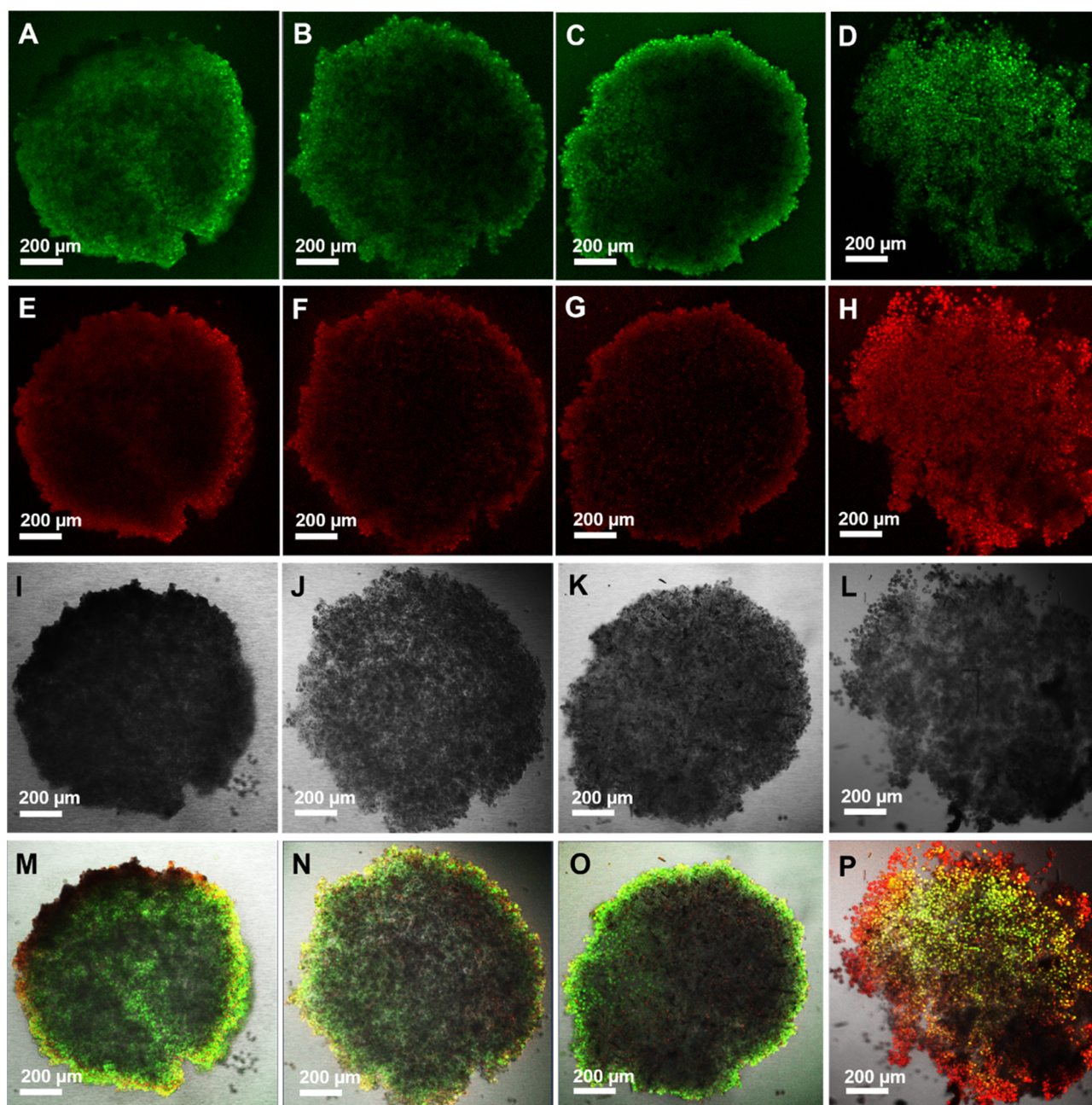


Figure 5. Live/dead cell staining assay. Confocal images of the AO-stained (A) control, (B) Cu-HXNP-treated, (C) quercetin-treated, and (D) quercetin-loaded Cu-HXNP-treated spheroid, showing green fluorescence. Confocal images of the PI-stained (E) control, (F) Cu-HXNP-treated, (G) quercetin-treated, and (H) quercetin-loaded Cu-HXNP-treated spheroid, showing red fluorescence. Corresponding bright field images of the (I) control, (J) Cu-HXNP-treated, (K) quercetin-treated, and (L) quercetin-loaded Cu-HXNP-treated spheroid. Merged images of the (M) control, (N) Cu-HXNP-treated, (O) quercetin-treated, and (P) quercetin-loaded Cu-HXNP-treated spheroid. The scale bar is 200 μm .

ions present on the planes of HXNPs.³⁴ The interaction of quercetin with Cu-HXNPs was confirmed by LCMS analysis. The LCMS spectrum of free quercetin (Figure S8A) showed an m/z value of 301.01, which was clearly evident in the quercetin-loaded Cu-HXNPs (Figure S8B), showing the presence of quercetin in Cu-HXNPs.^{35,36}

Using fluorescence spectroscopy, the loading efficiency was found to be 72% and the concentration of quercetin loaded within the Cu-HXNPs was thus calculated to be 3.6 mM. The cumulative release of quercetin from Cu-HXNPs at different time intervals was analyzed *in vitro* where maximum release was observed in an acidic environment (acetate buffer, pH 4)

as compared to the physiological environment (PBS buffer, pH 7.4). In pH 4, the release profile exhibited a slow and steady increase of drug release up to 12th h, where there occurred an initial burst release of 65% of drug with further 53% release at 24th h. Toward 48th h, the drug release was slowly declined, followed by displaying a steady pattern with 26% of drug release (Figure 2A). In pH 7.4, the release was suggested to be comparatively less with a maximum of 17% at 12th h followed by a gradual increase toward 48th h, showing 19% of release (Figure 2B). Thus, a pH-responsive release pattern could be observed with maximum release occurring in an acidic environment. Furthermore, by checking the release study up

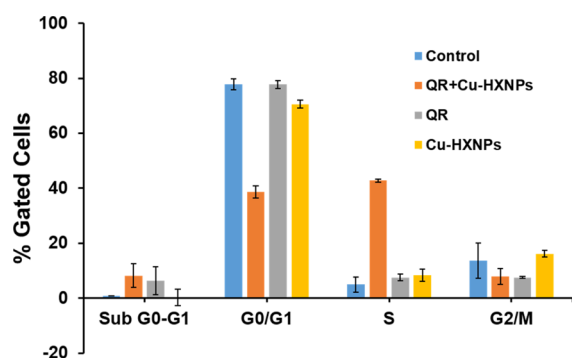


Figure 6. Cell cycle analysis of HeLa cells. The analysis was carried out for control cells and cells treated with quercetin-loaded Cu-HXNPs, free quercetin, and Cu-HXNPs.

to 96 h, it was confirmed that the release of total drug loaded might require more than 48 h, as there was 12 and 13% of quercetin released from quercetin loaded Cu-HXNPs at 72nd and 96th h, respectively, at pH 4 (Figure S9A). Similarly, at pH 7.4, a release of 19 and 20% of quercetin was observed at 72nd and 96th h, respectively (Figure S9B).

The uptake of quercetin-loaded Cu-HXNPs by HeLa cells was confirmed by confocal studies carried out at an excitation of 405 nm and at two different emission wavelengths (650 and 530 nm). In brief, Figure 3A depicts quercetin-loaded Cu-HXNP-treated HeLa cells at an emission of 650 nm which corresponds to CuNCs and Figure 3B depicts quercetin-loaded Cu-HXNP-treated HeLa cells at an emission of 530 nm that corresponds to quercetin. The representative bright-field image of HeLa cells treated with quercetin-loaded Cu-HXNPs is presented in Figure 3C. Figure 3D corresponds to the merged image of HeLa cells treated with quercetin-loaded Cu-HXNPs with emissions at 650 and 530 nm. The cellular intake of quercetin-loaded Cu-HXNPs was evident through the luminescence emitted from Cu-HXNPs and quercetin at their respective emission wavelength. The biocompatibility of HXNPs and the luminescence property of CuNCs can be contemplated as the attractive features in qualifying the entire nanof ormulation to be a suitable diagnostic probe in cancer theranostics. Similarly, the uptake of Cu-HXNPs (Figure S10A–D) and free quercetin (Figure S11A–D) was analyzed, and the images are given in the Supporting Information. The internalization of Cu-HXNPs and free quercetin by cells was clearly understood from the depth projection image of treated cells. Additionally, to explore the subcellular localization attribute of quercetin-loaded Cu-HXNPs, a cytopainter green lysosomal staining experiment was performed (Figure S12A–D). From the merged image of confocal microscopy obtained, it was revealed that the quercetin-loaded Cu-HXNPs were internalized and finally localized into lysosomal compartments (validated by the presence of yellow spots in the merged image, Figure S12D).

The cell viability study of quercetin-loaded Cu-HXNPs on HeLa cells was assessed by MTT assay through which their anticell proliferative efficiency was compared with only Cu-HXNPs and free quercetin. The MTT assay suggested that at 200 μM quercetin, the quercetin-loaded Cu-HXNPs exhibited IC_{50} , whereas free quercetin exhibited IC_{50} at 300 μM . In the case of only Cu-HXNPs, minimal killing was observed (Figure 4A). The MTT results suggest the ability of Cu-HXNPs to release quercetin, which could potentially enter the cells

bringing about conformational variations, propelling cell cycle modifications and apoptosis. Similarly, MTT assay was carried out for normal cell line such as HEK-293, which evinced negligible sensitivity toward free quercetin and Cu-HXNPs. At lower concentrations tested, the inhibitory action of quercetin-loaded Cu-HXNPs was found to be less on HEK-293 as compared to their action on HeLa. Toward the higher concentration of quercetin such as 500 μM , quercetin-loaded Cu-HXNPs gradually reduced the viability of HEK-293 cells to around 53% (Figure 4B).

The anticell proliferative activity in HeLa cells was found to be enhanced by the generation of ROS, which could be substantiated by DCFH-DA study (Figure 4C). In this study, we could confirm that there was an appreciable amount of ROS generated from cells treated with quercetin-loaded Cu-HXNPs in contrast to the control cells, which generated a minimal amount of ROS. At 200 μM , there was maximum generation of ROS by cells treated with quercetin-loaded Cu-HXNPs as compared to free quercetin and Cu-HXNPs. Quercetin is generally understood to be an antioxidant. However, studies suggest that flavonoids including quercetin can act as a pro-oxidant at its higher concentration and be driven to enhance the ROS production in the presence of transition metals such as copper. Now, our nanosystem such as Cu-HXNPs contains copper, which is a transition metal that is understood to initiate ROS formation through flavones.^{37,38} Thus, the ROS generation is probably intensified from the quercetin once it is successfully loaded into Cu-HXNPs and applied for the cellular treatment *in vitro*. Therefore, we suppose that under various conditions, quercetin tends to behave as an ambivalent compound, where it induces ROS generation rather than exhibiting the antioxidant property.³⁹ Through epifluorescence spectroscopy (Figure S13A–D), it was evident that the control cells emitted negligible DCF fluorescence, whereas cells treated with quercetin-loaded Cu-HXNPs emitted a considerable amount of DCF fluorescence due to the generation of ROS. This was in consonance with MTT assay, which suggested that the viability of cells was almost halved at 200 μM quercetin loaded in quercetin-loaded Cu-HXNPs with further reduction at higher concentration such as 500 μM quercetin. Generation of ROS could possibly play a major role in the reduction of cell proliferation where the cancer cells become more sensitive toward the enhanced intracellular ROS.⁴⁰

The 3D spheroids are understood to be better representative systems that mimic the *in vivo* tumor microenvironment.⁴¹ Therefore, the therapeutic ability of our present system on 3D spheroids was evaluated using alamarBlue-based viability assay. While analyzing the effect of quercetin-loaded Cu-HXNPs on 3D spheroids, approximately 50% of viability reduction was obtained at 500 μM quercetin up to which there was a gradual decrease in cell proliferation. With the increase in the concentration up to 1000 μM , the therapeutic effect of quercetin-loaded Cu-HXNPs on 3D spheroids was found to remain almost constant. The sensitivity of 3D spheroids toward free quercetin and Cu-HXNPs was milder in comparison to quercetin-loaded Cu-HXNPs (Figure 4D). To gain further insights into the efficiency of our present drug-loaded nanosystem, live/dead cell staining assay was carried out on the spheroids treated with Cu-HXNPs, free quercetin, and quercetin-loaded Cu-HXNPs (Figure 5A–P). As shown in Figure 5M–P, the untreated spheroid was found to have an intact morphology with significant green fluorescence due to

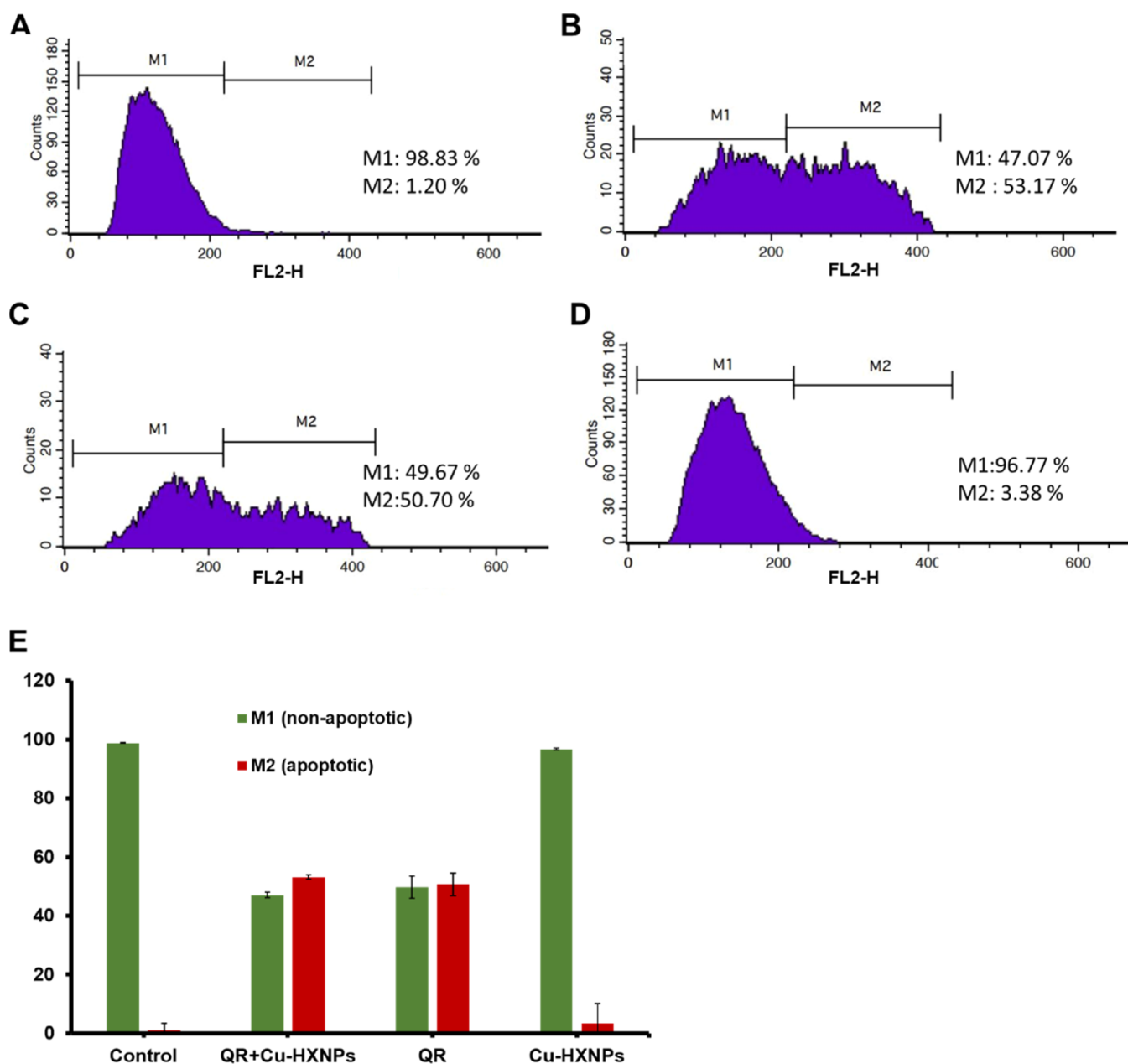


Figure 7. Cleaved caspase 3 assay for analyzing the percentage of apoptosis in HeLa cells. The figures represent results from (A) control, (B) quercetin-loaded Cu-HXNP, (C) free quercetin, and (D) Cu-HXNP treatments. (FL2-H represents the fluorescence signal height). (E) Graphical representation of assay showing M1 and M2 population of control and treated cells. The M1 population represents the nonapoptotic population, and M2 population represents the apoptotic population.

AO-stained live cells. The spheroid treated with free quercetin and Cu-HXNPs exhibited minimal disintegration and a minimum number of dead cells due to low fluorescence intensity emerging from red-emitting PI-stained cells. However, upon treatment with quercetin-loaded Cu-HXNPs, there was significant disintegration manifested in the entire spheroid with predominant red fluorescence emitted from a large number of PI-stained dead cells. Thus, the analysis suggests that Cu-HXNPs could successfully deliver quercetin deep within the spheroid, leading to appreciable disorganization of the 3D multicellular system.

Using FESEM analysis, the morphological evaluation of 2D monolayer culture of HeLa cells treated with quercetin-loaded Cu-HXNPs (200 μ M) was carried out, where the disrupted cell membrane was significantly evident as compared to the

untreated cells (Figure S14A,B). The mechanism behind such an alteration can be possibly due to the accumulation of ROS, which leads to disruption of protein and lipid bilayer, resulting in loss of cell membrane integrity. Moreover, ROS can act as common mediators of apoptosis, which is distinguished by morphological changes such as shrinkage, breakage, and blebbing of the membrane.^{42–44} This suggests quercetin-loaded Cu-HXNPs to be a suitable nanocarrier in bringing about significant intracellular changes that are partially manifested through morphological deformation of treated cells. When HEK-293 cell lines were treated with quercetin-loaded Cu-HXNPs at 200 μ M, no significant morphological changes were observed as compared to control cells, which implies the lower cytotoxic effect of the present drug-loaded

nanocarrier to normal cell lines in comparison to treated HeLa cells (Figure S15A,B).

The cell cycle study suggested the high anticell proliferative activity of quercetin-loaded Cu-HXNPs with the increase in the sub G_0/G_1 population (8.14%) compared to the control (0.73%) with subsequent changes in the other phases of the cell cycle such as G_0/G_1 , S, and G_2/M phases (Figure 6 and Figure S16A–D). The drug-treated cells also showed a slight increase in the sub G_0/G_1 population (6.25%) with changes in the other phases, whereas the only Cu-HXNP-treated cells exhibited similar cell population to that of the control in all the stages. We suppose that the action of quercetin released from quercetin-loaded Cu-HXNPs would have probably involved in the upregulation of tumor suppressor genes and down-regulation of genes involved in cell proliferation and differentiation.⁴⁵ The comparatively higher sub G_0/G_1 population in cells treated with quercetin-loaded Cu-HXNPs denotes the occurrence of apoptosis. Therefore, to confirm the apoptotic event, cleaved caspase 3-based assay was performed where the cells treated with quercetin-loaded Cu-HXNPs were found to have undergone apoptosis with the increase in the M2 population (53.17%) as compared to cells treated with free quercetin (50.70%). The apoptotic population found in the case of control cells was only 1.20%. In addition, the cells treated with only Cu-HXNPs did not exhibit significant apoptosis and was almost similar to control cells (Figure 7A–D, Table S1). A quantitative figure depicting the nonapoptotic and apoptotic population of control and treated HeLa cells is also included (Figure 7E). Thus, quercetin-loaded Cu-HXNPs are suggested to be potential in activating the caspase cascade, which could efficiently trigger the apoptosis process, inhibiting the further cell growth progression.

CONCLUSIONS

Briefly, Cu-HXNPs were synthesized and an anticancer drug quercetin was loaded for investigating the anticell proliferative activity as a nanocarrier. Cu-HXNPs were found to be efficient in loading the anticancer drug quercetin, which upon interacting with HeLa cells reduced their viability and survival. The quercetin-loaded Cu-HXNPs potentially modified the cell cycle pattern and induced apoptosis. Having the luminescent property, quercetin-loaded Cu-HXNPs exhibited the bioimaging property, which was found to be beneficial for confirming their cellular uptake. Upon checking with the normal cell line such as HEK-293, the present drug-loaded nanocarrier produced comparatively lower cytotoxicity with respect to HeLa cells. Interestingly, on analyzing the therapeutic significance of quercetin-loaded Cu-HXNPs on HeLa 3D spheroids, substantial disruption of the multicellular spheroid could be observed. Based on the performed studies and the subsequent outcome, we conclude that the formulated luminescent drug delivery vehicle has the potential to be explored wider for therapeutic and imaging application in the forthcoming cancer-related investigation.

ASSOCIATED CONTENT

Supporting Information

The Supporting Information is available free of charge at <https://pubs.acs.org/doi/10.1021/acsabm.1c00255>.

Fluorescence study, TEM analysis, FESEM, EDX, zeta potential analysis, LCMS, confocal microscopy, epifluor-

escence microscopy, and anticell proliferative studies (PDF)

AUTHOR INFORMATION

Corresponding Authors

Arun Chattopadhyay – Centre for Nanotechnology and Department of Chemistry, Indian Institute of Technology Guwahati, Guwahati 781039, India; orcid.org/0000-0001-5095-6463; Email: arun@iitg.ac.in

Siddhartha Sankar Ghosh – Centre for Nanotechnology and Department of Biosciences and Bioengineering, Indian Institute of Technology Guwahati, Guwahati 781039, India; orcid.org/0000-0002-7121-5610; Email: sghosh@iitg.ac.in

Authors

Anitha T. Simon – Centre for Nanotechnology, Indian Institute of Technology Guwahati, Guwahati 781039, India

Deepanjalee Dutta – Centre for Nanotechnology, Indian Institute of Technology Guwahati, Guwahati 781039, India; orcid.org/0000-0002-4695-5262

Complete contact information is available at: <https://pubs.acs.org/doi/10.1021/acsabm.1c00255>

Author Contributions

The manuscript was written through contributions of all authors. All authors have given approval to the final version of the manuscript.

Notes

The authors declare no competing financial interest.

ACKNOWLEDGMENTS

The authors gratefully acknowledge the financial support received from the Department of Electronics and Information Technology, Government of India (no. 5(9)/2012-NANO (vol. II)) and the Department of Biotechnology, Government of India (BT/PR13560/COE/34/44/2015 and BT/PR 25095/NER/95/1011/2017). A.C. thanks the Department of Science and Technology for the J. C. Bose Fellowship (JCB/2019/000039). We also acknowledge the instrument support from Centre for Nanotechnology, Centre for Environment (IIT Guwahati), and Central Instruments Facility (CIF, IIT Guwahati). Dr. Neha Arora, Dr. Bidkar Anil Parsram, Muktaashree Saha, (Department of Biosciences and Bioengineering, IIT Guwahati), Mihir Manna (Department of Chemistry, IIT Guwahati), and Debashree Debasmitta (Centre for Nanotechnology, IIT Guwahati) are also sincerely acknowledged for their valuable suggestions and timely help.

REFERENCES

- (1) Namiki, Y.; Fuchigami, T.; Tada, N.; Kawamura, R.; Matsunuma, S.; Kitamoto, Y.; Nakagawa, M. Nanomedicine for Cancer: Lipid-Based Nanostructures for Drug Delivery and Monitoring. *Acc. Chem. Res.* **2011**, *44*, 1080–1093.
- (2) Sun, Q.; Zhou, Z.; Qiu, N.; Shen, Y. Rational Design of Cancer Nanomedicine: Nanoproperty Integration and Synchronization. *Adv. Mater.* **2017**, *29*, 1606628.
- (3) Liu, Z.; Jiang, W.; Nam, J.; Moon, J. J.; Kim, B. Y. S. Immunomodulating Nanomedicine for Cancer Therapy. *Nano Lett.* **2018**, *18*, 6655–6659.
- (4) Jabr-Milane, L.; van Vlerken, L.; Devalapally, H.; Shenoy, D.; Komareddy, S.; Bhavsar, M.; Amiji, M. Multi-functional nanocarriers

- for targeted delivery of drugs and genes. *J. Controlled Release* **2008**, *130*, 121–128.
- (5) Björnmalm, M.; Thurecht, K. J.; Michael, M.; Scott, A. M.; Caruso, F. Bridging Bio-Nano Science and Cancer Nanomedicine. *ACS Nano* **2017**, *11*, 9594–9613.
- (6) Senapati, S.; Mahanta, A. K.; Kumar, S.; Maiti, P. Controlled drug delivery vehicles for cancer treatment and their performance. *Signal Transduction Targeted Ther.* **2018**, *3*, 7.
- (7) Munir, M. U.; Ihsan, A.; Javed, I.; Ansari, M. T.; Bajwa, S. Z.; Bukhari, S. N. A.; Ahmed, A.; Malik, M. Z.; Khan, W. S. Controllably Biodegradable Hydroxyapatite Nanostructures for Cefazolin Delivery against Antibacterial Resistance. *ACS Omega* **2019**, *4*, 7524–7532.
- (8) Sau, T. K.; Rogach, A. L.; Jäckel, F.; Klar, T. A.; Feldmann, J. Properties and applications of colloidal nonspherical noble metal nanoparticles. *Adv. Mater.* **2010**, *22*, 1805–1825.
- (9) Geuli, O.; Miller, M.; Leader, A.; He, L.; Melamed-Book, N.; Tshuva, E. Y.; Reches, M.; Mandler, D. Electrochemical Triggered Dissolution of Hydroxyapatite/Doxorubicin Nanocarriers. *ACS Appl. Bio Mater.* **2019**, *2*, 1956–1966.
- (10) Qi, C.; Zhu, Y.-J.; Lu, B.-Q.; Zhao, X.-Y.; Zhao, J.; Chen, F. Hydroxyapatite nanosheet-assembled porous hollow microspheres: DNA-templated hydrothermal synthesis, drug delivery and protein adsorption. *J. Mater. Chem.* **2012**, *22*, 22642–22650.
- (11) Dasgupta, A.; Biancacci, I.; Kiessling, F.; Lammers, T. Imaging-assisted anticancer nanotherapy. *Theranostics* **2020**, *10*, 956–967.
- (12) Bai, X.; Wang, S.; Xu, S.; Wang, L. Luminescent nanocarriers for simultaneous drug or gene delivery and imaging tracking. *Trac. Trends Anal. Chem.* **2015**, *73*, 54–63.
- (13) Bhattacharyya, K.; Mukherjee, S. Fluorescent Metal Nano-Clusters as Next Generation Fluorescent Probes for Cell Imaging and Drug Delivery. *Bull. Chem. Soc. Jpn.* **2018**, *91*, 447–454.
- (14) Tao, Y.; Li, M.; Ren, J.; Qu, X. Metal nanoclusters: novel probes for diagnostic and therapeutic applications. *Chem. Soc. Rev.* **2015**, *44*, 8636–8663.
- (15) Ghosh, R.; Goswami, U.; Ghosh, S. S.; Paul, A.; Chattopadhyay, A. Synergistic anticancer activity of fluorescent copper nanoclusters and cisplatin delivered through a hydrogel nanocarrier. *ACS Appl. Mater. Interfaces* **2015**, *7*, 209–222.
- (16) Simon, A. T.; Dutta, D.; Chattopadhyay, A.; Ghosh, S. S. Copper Nanocluster-Doped Luminescent Hydroxyapatite Nanoparticles for Antibacterial and Antibiofilm Applications. *ACS Omega* **2019**, *4*, 4697–4706.
- (17) Hu, K.; Miao, L.; Goodwin, T. J.; Li, J.; Liu, Q.; Huang, L. Quercetin Remodels the Tumor Microenvironment To Improve the Permeation, Retention, and Antitumor Effects of Nanoparticles. *ACS Nano* **2017**, *11*, 4916–4925.
- (18) Srivastava, S.; Somasagara, R. R.; Hegde, M.; Nishana, M.; Tadi, S. K.; Srivastava, M.; Choudhary, B.; Raghavan, S. C. Quercetin, a Natural Flavonoid Interacts with DNA, Arrests Cell Cycle and Causes Tumor Regression by Activating Mitochondrial Pathway of Apoptosis. *Sci. Rep.* **2016**, *6*, 24049.
- (19) Hashemzaei, M.; Far, A. D.; Yari, A.; Heravi, R. E.; Tabrizian, K.; Taghdisi, S. M.; Sadegh, S. E.; Tsarouhas, K.; Kouretas, D.; Tzanakakis, G.; Nikitovic, D.; Anisimov, N. Y.; Spandidos, D. A.; Tsatsakis, A. M.; Rezaee, R. Anticancer and apoptosis-inducing effects of quercetin in vitro and in vivo. *Oncol. Rep.* **2017**, *38*, 819–828.
- (20) Syamchand, S. S.; Sony, G. Multifunctional hydroxyapatite nanoparticles for drug delivery and multimodal molecular imaging. *Microchim. Acta* **2015**, *182*, 1567–1589.
- (21) Weerasuriya, D. R. K.; Wijesinghe, W. P. S. L.; Rajapakse, R. M. G. Encapsulation of anticancer drug copper bis(8-hydroxyquinoline) in hydroxyapatite for pH-sensitive targeted delivery and slow release. *Mater. Sci. Eng., C* **2017**, *71*, 206–213.
- (22) Chen, M.-H.; Hanagata, N.; Ikoma, T.; Huang, J.-Y.; Li, K.-Y.; Lin, C.-P.; Lin, F.-H. Hafnium-doped hydroxyapatite nanoparticles with ionizing radiation for lung cancer treatment. *Acta Biomater.* **2016**, *37*, 165–173.
- (23) Wang, H.; He, L.; Zhang, P.; Zhang, J.; Chen, Z.; Ren, X.; Mei, X. Folate-modified hydroxyapatite nanorods induce apoptosis in MCF-7 cells through a mitochondrial-dependent pathway. *New J. Chem.* **2019**, *43*, 14728–14738.
- (24) Ikeda, N. E. A.; Novak, E. M.; Maria, D. A.; Velosa, A. S.; Pereira, R. M. S. Synthesis, characterization and biological evaluation of Rutin-zinc(II) flavonoid-metal complex. *Chem. Biol. Interact.* **2015**, *239*, 184–191.
- (25) Zhao, H.; Wu, C.; Gao, D.; Chen, S.; Zhu, Y.; Sun, J.; Luo, H.; Yu, K.; Fan, H.; Zhang, X. Antitumor Effect by Hydroxyapatite Nanospheres: Activation of Mitochondria-Dependent Apoptosis and Negative Regulation of Phosphatidylinositol-3-Kinase/Protein Kinase B Pathway. *ACS Nano* **2018**, *12*, 7838–7854.
- (26) Wang, J.; Zhang, X.; Li, X.; Zhang, Y.; Hou, T.; Wei, L.; Qu, L.; Shi, L.; Liu, Y.; Zou, L.; Liang, X. Anti-gastric cancer activity in three-dimensional tumor spheroids of bufadienolides. *Sci. Rep.* **2016**, *6*, 24772.
- (27) Patra, M.; Mukherjee, R.; Banik, M.; Dutta, D.; Begum, N. A.; Basu, T. Calcium phosphate-quercetin nanocomposite (CPQN): A multi-functional nanoparticle having pH indicating, highly fluorescent and anti-oxidant properties. *Colloids Surf., B* **2017**, *154*, 63–73.
- (28) Mezzetti, A.; Protti, S.; Lapouge, C.; Cornard, J.-P. Protic equilibria as the key factor of quercetin emission in solution. Relevance to biochemical and analytical studies. *Phys. Chem. Chem. Phys.* **2011**, *13*, 6858–6864.
- (29) Chen, Z.; Qian, S.; Chen, J.; Chen, X. Highly fluorescent gold nanoclusters based sensor for the detection of quercetin. *J. Nanopart. Res.* **2012**, *14*, 1264.
- (30) Oliveira, E.; Bértolo, E.; Núñez, C.; Pilla, V.; Santos, H. M.; Fernández-Lodeiro, J.; Fernández-Lodeiro, A.; Djafari, J.; Capelo, J. L.; Lodeiro, C. Green and Red Fluorescent Dyes for Translational Applications in Imaging and Sensing Analytes: A Dual-Color Flag. *ChemistryOpen* **2018**, *7*, 9–52.
- (31) Farzadi, A.; Bakhshi, F.; Solati-Hashjin, M.; Asadi-Eydivand, M.; Osman, N. A. a. Magnesium incorporated hydroxyapatite: Synthesis and structural properties characterization. *Ceram. Int.* **2014**, *40*, 6021–6029.
- (32) Lin, K.; Liu, X.; Chang, J.; Zhu, Y. Facile synthesis of hydroxyapatite nanoparticles, nanowires and hollow nano-structured microspheres using similar structured hard-precursors. *Nanoscale* **2011**, *3*, 3052–3055.
- (33) Sheikh, F. A.; Kanjwal, M. A.; Macossay, J.; Barakat, N. A. M.; Kim, H. Y. A simple approach for synthesis, characterization and bioactivity of bovine bones to fabricate the polyurethane nanofiber containing hydroxyapatite nanoparticles. *eXPRESS Polym. Lett.* **2012**, *6*, 41–53.
- (34) Okada, M.; Matsumoto, T. Synthesis and modification of apatite nanoparticles for use in dental and medical applications. *Jpn. Dent. Sci. Rev.* **2015**, *51*, 85–95.
- (35) Vacek, J.; Papoušková, B.; Vrba, J.; Zatloukalová, M.; Křen, V.; Ulrichová, J. LC-MS metabolic study on quercetin and taxifolin galloyl esters using human hepatocytes as toxicity and biotransformation in vitro cell model. *J. Pharm. Biomed. Anal.* **2013**, *86*, 135–142.
- (36) Tanaka, S.; Trakooncharoenvit, A.; Nishikawa, M.; Ikushiro, S.; Hara, H. Comprehensive Analyses of Quercetin Conjugates by LC/MS/MS Revealed That Isorhamnetin-7-O-glucuronide-4'-O-sulfate Is a Major Metabolite in Plasma of Rats Fed with Quercetin Glucosides. *J. Agric. Food Chem.* **2019**, *67*, 4240–4249.
- (37) Galluzzo, P.; Martini, C.; Bulzomi, P.; Leone, S.; Bolli, A.; Pallottini, V.; Marino, M. Quercetin-induced apoptotic cascade in cancer cells: Antioxidant versus estrogen receptor α -dependent mechanisms. *Mol. Nutr. Food Res.* **2009**, *53*, 699–708.
- (38) Cao, G.; Sofic, E.; Prior, R. L. Antioxidant and prooxidant behavior of flavonoids: structure-activity relationships. *Free Radic. Biol. Med.* **1997**, *22*, 749–760.
- (39) De Marchi, U.; Biasutto, L.; Garbisa, S.; Toninello, A.; Zoratti, M. Quercetin can act either as an inhibitor or an inducer of the mitochondrial permeability transition pore: A demonstration of the ambivalent redox character of polyphenols. *Biochim. Biophys. Acta, Bioenerget.* **2009**, *1787*, 1425–1432.

(40) Dharmaraja, A. T. Role of Reactive Oxygen Species (ROS) in Therapeutics and Drug Resistance in Cancer and Bacteria. *J. Med. Chem.* **2017**, *60*, 3221–3240.

(41) Edmondson, R.; Broglie, J. J.; Adcock, A. F.; Yang, L. Three-dimensional cell culture systems and their applications in drug discovery and cell-based biosensors. *Assay Drug Dev. Technol.* **2014**, *12*, 207–218.

(42) Perillo, B.; Di Donato, M.; Pezone, A.; Di Zazzo, E.; Giovannelli, P.; Galasso, G.; Castoria, G.; Migliaccio, A. ROS in cancer therapy: the bright side of the moon. *Exp. Mol. Med.* **2020**, *52*, 192–203.

(43) Redza-Dutordoir, M.; Averill-Bates, D. A. Activation of apoptosis signalling pathways by reactive oxygen species. *Biochim. Biophys. Acta* **2016**, *1863*, 2977–2992.

(44) Rameshthangam, P.; Chitra, J. P. Synergistic anticancer effect of green synthesized nickel nanoparticles and quercetin extracted from *Ocimum sanctum* leaf extract. *J. Mater. Sci. Technol.* **2018**, *34*, 508–522.

(45) Bishayee, K.; Ghosh, S.; Mukherjee, A.; Sadhukhan, R.; Mondal, J.; Khuda-Bukhsh, A. R. Quercetin induces cytochrome-c release and ROS accumulation to promote apoptosis and arrest the cell cycle in G2/M, in cervical carcinoma: signal cascade and drug-DNA interaction. *Cell Prolif* **2013**, *46*, 153–163.